# Design, Fabrication, and Testing of an Electrohydrodynamic Ion-Drag Micropump

Jeff Darabi, *Member, IEEE*, Mihai Rada, Michael Ohadi, and John Lawler

***Abstract*—This paper presents the design, fabrication, and testing of a novel electrohydrodynamic (EHD) ion-drag micropump. In order to maximize the electrical field gradients that are responsible for EHD pumping, we incorporated three-dimensional (3-D) triangular bumps of solder as part of the EHD electrodes. To form these bumps, Niobium was sputter-deposited onto a ceramic substrate, coated with photoresist, optically exposed and etched using a reactive ion etcher to define the electrode pattern. The substrate was then "dipped" into a molten solder pool. Since the solder adheres only to the metallic film, bumps of solder form on the electrodes, giving the electrodes a significant 3-D character. The overall dimensions of the micropump are 19 mm $\times$ 32 mm $\times$ 1.05 mm. Four different designs were fabricated and tested. Static pressure tests were performed with a 3M Thermal Fluid (HFE-7100) as the working fluid and the optimum design was identified. The results with the thermal fluid were highly promising and indicated a pumping head of up to 700 Pa at an applied voltage of 300 V. The experimental results for the four different designs show that the presence of the 3-D bump structures significantly improves the pumping performance. Also, a much better pumping performance was obtained with the micropump in which the emitter had a saw-tooth shape. [816]**

***Index Terms*—Electrohydrodynamics (EHDs), ion-drag, micropump, three-dimensional (3-D) electrode.**

## I. Introduction

THE electrohydrodynamic (EHD) pumping uses the interaction of an electric field with electric charges, dipoles or particles embedded in a dielectric fluid to move the fluid. The charges can be injected directly by sharp points or by special means such as adding a small amount of a liquid containing a high density of ions. The major driving force in ion drag pumps is the movement of ions across an imposed electric field. The electric field is established between a charged electrode called an emitter and a grounded electrode called a collector. If an electrical field is strong enough, the electrons that are normally present in the liquid from ionized molecules can be accelerated to ionize other molecules. The electrons, accelerated to a high speed, will act as ion producers. The Coulomb force that is produced by an external electrical field affects all the charges in the fluid. The resulting net force that acts on the electrons and ions is the same. However, since the mass of the electron is negligible compared to the mass of the ion, the major impact on the fluid motion is produced by the motion of the ions [1]. The friction between the moving ions and the working fluid drags the working fluid toward the collector, thus setting the fluid (both charged and uncharged species) in motion. Two of the most important aspects of ion-drag pumping are the design of the electrodes and the existence of sharp points on the emitter electrodes at which charge injection occurs. The electric field can be generated with a variety of electrode configurations, including transverse mesh electrodes, needle or parallel electrodes, longitudinal traveling-wave electrodes and many others.

The fact that dielectric liquids can be pumped by the injection of ions in an applied electric field has been known for quite some time. Indeed, the theoretical and experimental investigations of the EHD pump were widely pursued in early 1960's. Stuetzer [1] and Pickard [2] were among the first who proposed and studied the ion-drag EHD pump. Later, many researchers [3]–[5] made further studies of the ion-drag EHD pump. Using a simplified model, Stuetzer [1] arrived at the following relation between pressure and electric field intensity:

$$P(x) - P_0 = \frac{\varepsilon}{2}\left(E(x)^2 - E_0^2\right) \tag{1}$$

where $P$ is the pressure within the fluid, $E$ the electric field intensity and $\varepsilon$ the permittivity. The basic assumption in deriving the above equation was to use two plane-parallel electrodes to approximate the wire grid electrodes in practice. This means that the variation of charge density around point-shaped emitter was neglected. Stuetzer [1] derived the maximum static pressure obtainable from a dielectric liquid and ion drag pump with plane electrode as:

$$P_{\max} = \frac{9}{8}\varepsilon \cdot \left(\frac{V - V_0}{d}\right)^2 \tag{2}$$

where $V_0$ is the threshold voltage below which no pressure is obtainable and $d$ is the spacing between the electrodes. Pickard [2] arrived at a slightly different relation for EHD pumping:

$$P_{\max} = \frac{9}{8}\eta\varepsilon \cdot \left(\frac{V}{d}\right)^2 \tag{3}$$

where $\eta$, bounded between 0 and 1, is a coefficient which takes into account the influence of several factors, mainly the charge emission laws at the electrodes.

An improved model of the EHD pumping by Crowley [6] introduced a basic understanding of ion-drag force from an elec-

Manuscript received February 15, 2002; revised May 29, 2002. This work was supported by the Advanced Thermal and Environmental Concepts, Inc. (ATEC, Inc., College Park, MD) through a sub-contract for a project funded by the Office of Naval Research. Subject Editor C.-J. Kim.

J. Darabi is with the Department of Mechanical Engineering, University of South Carolina, Columbia, SC, 29208 USA (e-mail: darabi@engr.sc.edu).

M. Rada and M. Ohadi are with the University of Maryland, College Park, MD.

J. Lawler is with the ATEC, Inc., College Park, MD.

Digital Object Identifier 10.1109/JMEMS.2002.805046

1057-7157/02$17.00 © 2002 IEEE

trostatics point of view. He developed the following relations for a force density and a maximum pressure inside ion-drag pump:

$$F = \frac{\rho_0 V_0}{d} + \frac{\rho_0^2}{\varepsilon}\left(x - \frac{d}{2}\right) \quad (4)$$

$$P_{\max} = 2\varepsilon \cdot \left(\frac{V}{d}\right)^2 \quad (5)$$

It should be noted that the maximum pressure given by (5) is much larger than that predicted by Stuetzer [1] via (2) and Packard [2] via (3). Equation (5) is only an approximation, since many assumptions, including the presence of a uniform electric field, were made. In practice, the electric field is distorted, which makes predicting the performance of pumps containing electrodes with sharp features (required for good pumping) more complicated. For example, (4) indicates that a nonuniform pressure will exist within a fluid because of the EHD force, $F$, varies with the fluid's distance $x$ from the emitter. This force gradient can generate an internal stirring of the fluid, forming electroconvection, which can reduce the output pressure.

The driving force of an ion drag pump is the Coulomb force, thus its pumping performance relies critically on the electric properties of the liquids, such as permittivity ($\varepsilon$), conductivity ($\sigma$) and viscosity ($\mu$). Generally, high permittivity and low viscosity are required for high pumping performance. Crowley [1] showed that high dielectric constant and low viscosity would lead to high flow velocity, while low electric conductivity and mobility would promote high efficiency. The flow rate $u$ and pressure $p$ are expected to show quadratic increases with applied voltage.

With the development of microfabrication technology, intense research efforts have been made toward microfluidic systems and microliquid handling devices. In microfabricated systems, pumps without moving parts are of special interest. EHD pumps produce no vibration, require low power consumption, are electronically controllable and require no or little maintenance. These advantages make them attractive for applications in microsystems. The efficiency of an EHD pump is rather low, but this drawback can be offset by other benefits of EHD pumping such as the freedom from moving parts. The use of the electrohydrodynamic technique for micro-scale fluid pumping has been investigated by a number of researchers over the past decade [7]–[11]. Potential applications of EHD micropumps include: pumping and portioning of minute quantities of a large variety of fluids, implantable medicine dosage control, fuel injection, microscopic fluid or gas sampling and integrated cooling devices.

Bart *et al.* [7] discloses an EHD pumping principle employing a traveling electrical wave or charge imposed between electrodes positioned in a substantially parallel array whereby a nonelectrically conducting fluid is moved transverse to the electrodes by a sinusoidally applied voltage. This micropump consisted of 10 $\mu$m parallel electrodes spaced 10 $\mu$m apart and 1.75 $\mu$m thick. The electrodes were connected to allow the generation of a three-phase electric wave. No pumping data was documented there. Richter *et al.* [8] proposed a micromachined ion-drag EHD pump, consisting of pairs of facing permeable or perforated substantially planar grids through which the pumped fluid moves. Richter displays an array of pairs for increasing the pumping head. The gap of the grid electrodes is 350 $\mu$m. A maximum static pressure of 2500 Pa and a pumping rate of 14 mL/min have been achieved for ethanol. The applied voltage is about 500 V. Its flow rate is almost three orders of magnitude higher than that of piezoelectric or thermally excited micropump.

Fuhr *et al.* [9] uses a traveling wave pumping design and suggests that a square wave format is superior to sinusoidal wave format. He employs a grid of microelectrodes and uses a single phase or poly-phase electrical alternating potential applied to his electrodes. He further points out that traveling wave pumping principles require that the fluid pumped exhibit a gradient in the properties of electrical conductivity or permittivity.

Ahn [10] fabricated an ion-drag micropump that consisted of planar electrodes in a 3 mm wide channel with a channel height of 200 $\mu$m. Ethyl alcohol was used as the working fluid. A flow arte of 55 $\mu$L/min was documented at an applied voltage of 60 V.

Darabi *et al.* [11] developed a polarization micropump for microelectronics cooling applications. The device incorporated an active evaporative cooling surface, a polarization micropump and temperature sensors into a single chip. The prototype device demonstrated a maximum cooling capacity of 65 W/cm$^2$ with a corresponding pumping head of 250 Pa.

In an ion-drag pump, the pumping is achieved if the electrical shear stresses are higher than the viscous shear stresses. Thus, the locations at which ions are generated and to which they are accelerated play an important role in determining the overall pumping efficiency, so the design of the electrode pair is of crucial importance. However, very few studies have been conducted on this topic at the micro scale. The simplest arrangement is to use a series of planar comb finger electrodes, often called emitters and collectors and allow the liquid to flow through them. However, very few experimental studies of these "simple" pumps fabricated at the micro-scale have been published, so the design rules or optimized designs for these micro pumps have not been established. In the present investigation, we compared the pumping performance of various two- and three-dimensional (3-D) electrode features in order to begin to develop some of these design rules for maximizing the pumping performance of EHD ion-drag micropumps.

## II. Design and Fabrication

We designed an ion-drag EHD pump that employs a series of electrodes with the different 3-D features that maximize the field gradients responsible for electrohydrodynamic (EHD) pumping. The micropump is made from three pieces that are bonded together. The bottom substrate and the top cover are alumina substrates and the sidewall consists of an epoxy gasket. The electrodes are deposited on the bottom substrate. A laser was used to cut inlet and outlet ports into the top cover. The main components of the micropump are shown in Fig. 1. They are as follows.

- A ceramic (alumina) substrate on which a set of EHD electrodes are deposited and patterned. The designs consist of planar and saw-tooth emitters and planar collectors. The

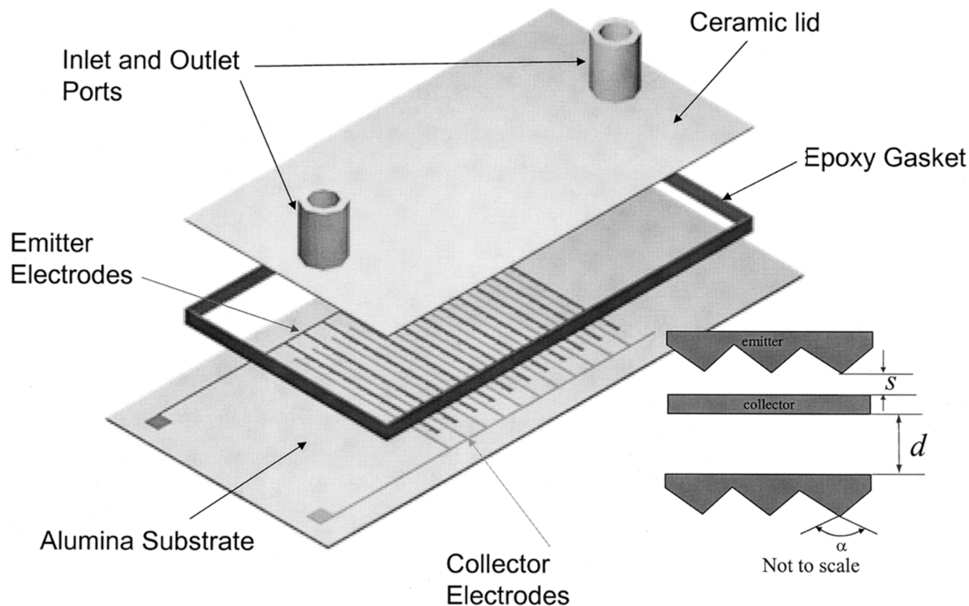


Fig. 1. Schematic diagram of the micropump.

electrical connection leads are passed beneath the epoxy side wall and wire bonded to the external leads.
- An epoxy gasket (side wall).
- A top cover with inlet and outlet ports.

### A. Emitter and Collector Patterns

The electrode geometry and dimensions have been carefully selected to allow a wide range of test conditions. Four different electrode patterns were designed. The distances between the emitter and collector electrodes ($s$) as well as the distances between the stages ($d$) are varied in the different layouts. The saw-tooth pattern was designed to produce a more intense field at the tip of the emitter, resulting in a higher charge injection. The collector electrode consists of a planar strip with a width of 10 $\mu$m. The base width of the emitter electrodes is 10 $\mu$m. The base length of a saw-tooth is 20 $\mu$m with a 60°-tip angle.

The first electrode layout, labeled A1, consists of planar emitters and collectors. The electrode gap is 50 $\mu$m and the distance between stages is 100 $\mu$m. The second design (A2) has an electrode gap of 50 $\mu$m with a 100 $\mu$m distance between stages. In this design, the emitter has a saw-tooth geometry to provide higher field intensities gradients, resulting in a higher pumping at lower voltages. The third design (B1) presents a saw-tooth design and has a higher electrode gap of 100 $\mu$m with a 200 $\mu$m distance between the stages. This design along with the A2 design will allow us to study the effect of the electrode gap for the saw-tooth geometry. The fourth design (B2) is similar to the previous design with the inclusion of 3D bump structures along the emitter electrode. The solder bumps with diameters ranging between 4 micrometer and 1 mm can be produced with a bump height approximately 12% of the base diameter. The surface shape depends on the base geometry and it is very complicated for noncircular geometries. For round bumps, however, the surface shape is a slice of a sphere. The bumps were placed on every other saw-tooth. The fact that the ions are injected in the region away from the wall should further increase the pumping efficiency. This design in conjunction with the B1 design will allow us to study the effect of the 3D bump structures on the pumping. The specifications of the four different designs are summarized in Table I.

TABLE I
SPECIFICATIONS OF VARIOUS ELECTRODE DESIGNS (SEE FIG. 1)

| Design Option | Geometry | S (μm) | d (μm) | Emitter tip angle (α - degrees) | No. of stages |
|---|---|---|---|---|---|
| A1 | Planar | 50 | 100 | N/A | 95 |
| A2 | Saw-tooth | 50 | 100 | 60 | 80 |
| B1 | Saw-tooth | 100 | 200 | 60 | 50 |
| B2 | Saw-tooth with bumps | 100 | 200 | 60 | 50 |

### B. Microfabrication

Fabrication began with polished alumina substrates. The substrates were approximately 3-inch square, allowing six units to be fabricated in parallel. Niobium metallization was sputter-deposited onto the ceramic, coated with photoresist and optically exposed using a 1X aligner. Following development, a reactive ion etch defined the niobium metallization pattern. Half of the designs used a titanium/paladium/gold (Ti/Pd/Au) overlayer, capable of accepting solder. Niobium provides an electrical connection between individual solder bumps. A liftoff pattern of photoresist was deposited, exposed and developed. Ti/Pd/Au was sequentially evaporated in 40/400/40 nanometer thicknesses. Rinsing off the remaining photoresist left Ti/Pd/Au behind on the chosen regions of the niobium. The three metals served three different functions: a 35-nm high Ti layer was used as an adhesive/barrier layer, a 400-nm Pd layer was used as a contact layer and a 50-nm Au layer prevented Pd oxidation. These layers are schematically shown in Fig. 2. A solder dipping process deposited InSn solder onto the Ti/Pd/Au patterns; the solder forming rounded bumps on the regions containing the Ti/Pd/Au layers. Microscope photos of the electrode structures are shown in Fig. 3. The advantage

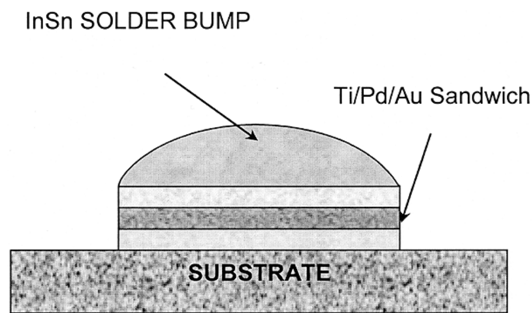


Fig. 2. Schematic diagram of 3-D bump structures.

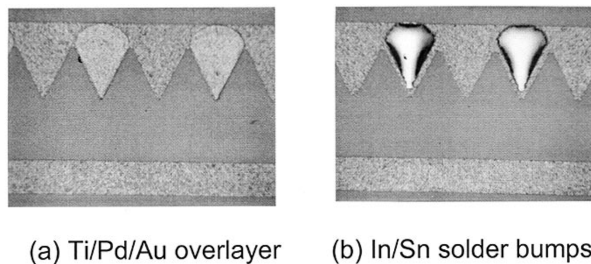


Fig. 3. Microscope photos of electrode structures. (a) Ti/Pd/Au overlayer and (b) In/Sn solder bumps.

of this process is that complex microstructures can be produced using a series of simple steps.

The top covers consisted of the same ceramic material as the base. Laseronics Corporation used a laser to cut the ceramic to the correct final dimensions and to include an inlet and outlet port onto each cover. Assembly was completed with an epoxy film to create the cavity sidewalls. The individual bottoms and covers were aligned with an epoxy gasket. Under pressure and with heating (150°C), the epoxy was cured for an hour. The epoxy thickness (channel height) was measured after the assembly and found to be between 40 $\mu$m–70 $\mu$m. The range in numbers indicates a degree of tilt after assembly.

## III. Experimental Setup

The first static pumping tests were performed using a 3M's HFE-7100 heat transfer fluid. This fluid has a low vapor pressure; hence, it does not require a high-pressure closed-loop system. Also, it has a good dielectric constant, $k \sim 7.4$, a relatively low viscosity and a relatively high thermal conductivity. The boiling point of HFE-7100 fluid is 61°C at atmospheric pressure. Other thermo-physical properties of this fluid are listed in Table II.

The device (without inlet and outlet ports) is shown in Fig. 4. Each device measures 19 mm × 32 mm × 1.05 mm. The tests were performed in a transparent glass container. In order to test the pumping capability of the device, a glass tube was mounted on the exit port of these devices using transparent epoxy. The device was placed in a bath of a 3M thermal fluid and a negative dc voltage was applied to the emitter electrodes and collector electrodes were grounded. A 0–1000 V dc power supply with a

TABLE II
Thermophysical Properties of HFE-7100 Fluid

| Thermophysical Property | HFE-7100 |
|---|---|
| Boiling Point (°C) (at 1 atm) | 61 |
| Liquid density (kg/m$^3$) | 1402 |
| Liquid kinematic viscosity (cSt ) | 0.38 |
| Liquid specific heat (J/kg-K ) | 1253 |
| Dielectric strength (kV/mm ) | 11 |
| Dielectric constant | 7.40 |

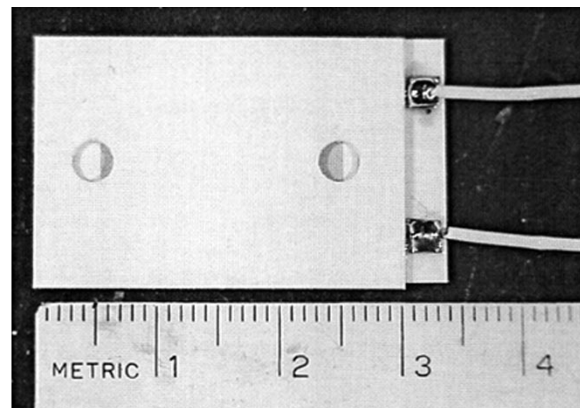


Fig. 4. A photograph of the assembled micropump.

Fig. 5. Static pressure test of device (Liquid column level is near the top of tube).

resolution of 1 V and 1 $\mu$A was used to provide the necessary voltage to the EHD pump.

As shown in Fig. 5, the pump produced a liquid column rise of about 45 mm, which corresponds to over 600 Pa pressure. As the voltage was further increased to 700 V (for a 100 $\mu$m electrode gap), the liquid overflowed the 45 mm tube. When a longer tube was used, the pump produced a liquid rise of about 53 mm corresponding to 780 Pa pressure. These results were highly promising and demonstrated successfully the pumping capabilities of the micropump.

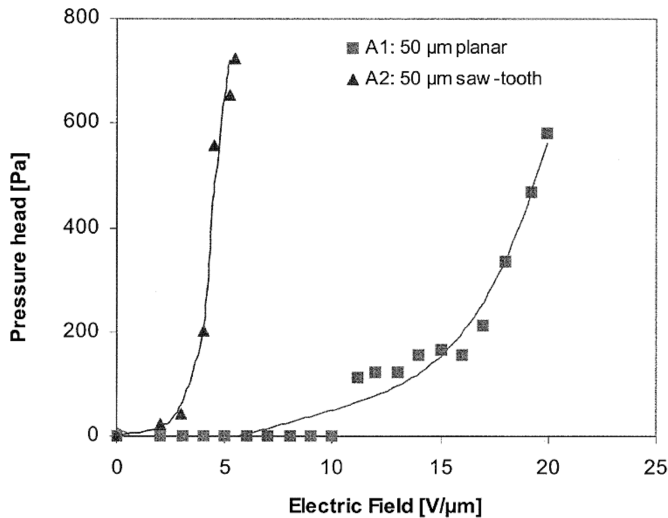


Fig. 6. Pressure head versus electric field for the 50 $\mu$m planar and saw-tooth designs.

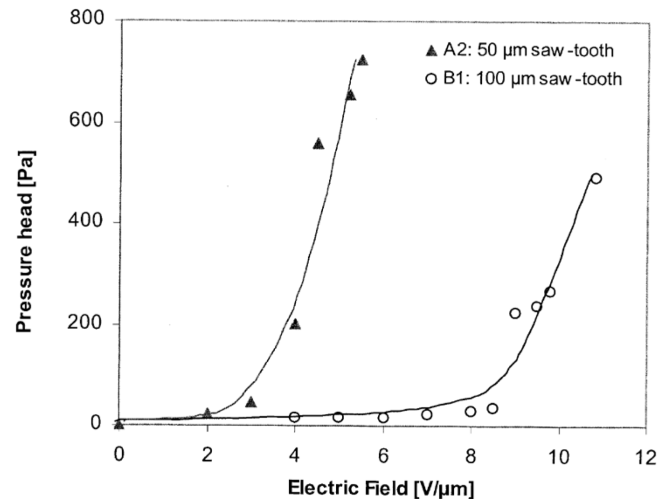


Fig. 7. Pressure head versus electric fields strength for two different electrode gaps.

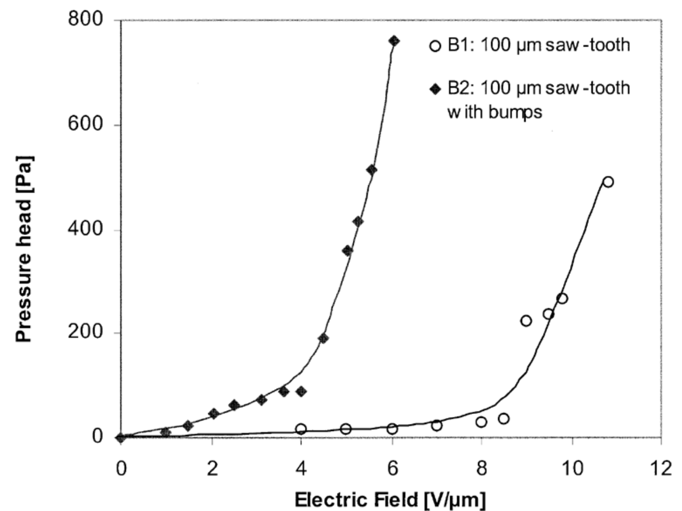


Fig. 8. Pressure head versus electric field for 100 $\mu$m saw-tooth electrode with and without 3D bumps on the electrodes.

## IV. Experimental Results

The pumping experiments were performed with these four modules using the 3M's HFE-7100 as the working liquid. The transparent container and the test module were carefully cleaned with acetone to avoid the contamination of the fluid with impurities. Then the test device was fixed on the bottom of the transparent container and the electrical connections to the power supply were made. The container was then filled with the 3M fluid to a reference level. The reference level was recorded. The voltage was applied to the electrodes and the liquid height rise was recorded. The liquid column level was relatively stable over a period of 2 hours. However, a slight fluctuation in the liquid level was observed. A work is in progress to address the long-term performance.

The pumping head results for the planar and saw-tooth geometry are shown in Fig. 6. The electrode gap in both cases is 50 $\mu$m. The results clearly show a much higher pumping performance with the saw tooth geometry as compared to the planar electrode. Although the electrode gap is the same in both cases, the pumping starts at a much higher voltage for the planar electrode. For the planar geometry, approximately 900 V is required to produce a pumping head of 600 Pa, whereas only 200 V is required with the saw-tooth geometry. It is believed that this is due the higher electric field gradient for the saw-tooth design, which facilitates the ion injection process, resulting in a higher pumping efficiency.

The results obtained with the saw-tooth electrodes for electrode gaps of 50 $\mu$m and 100 $\mu$m are shown in Fig. 7. We believe the larger number of stages (pairs of electrodes) in the 50 $\mu$m-gap device is responsible for the better pumping performance of this design.

The pumping head results for the 100 $\mu$m saw-tooth design with and without 3-D bump structures are shown in Fig. 8. The results show that the pumping effect is significantly improved by the presence of the bump structures. This observation is likely due to the ions being injected further away from the wall for the bump electrode and thus, allowing a more efficient momentum transfer to the bulk of the fluid. It can be seen that for the no bump geometry, a pumping head of 500 Pa is obtained at a voltage of 1000 V, whereas this same pumping head can be obtained for the bump geometry at less than 500 V.

The experimental results for the four different designs are presented in Fig. 9. Several observations can be made from these graphs. As expected the planar design (A1) has the lowest performance. The second observation is that a much higher pumping performance can be obtained with the design with saw-tooth emitters. The pumping head results obtained with the B2 design show that the presence of the 3D bump structures significantly improved the pumping performance. Among the four electrode geometries tested, the A2 design, which has a larger number of pumping stages, performed the best. Along with the progress in micro fabrication technologies, the space between the emitter electrode and the collector electrode in an electrical field can be reduced to the range from 10 to 50 $\mu$m and the operating voltage can be lower than 200 V. Thus, reducing the electrode gap and increasing the number of pumping stages can significantly improve the pumping capability. Also, the results clearly show that the 100-$\mu$m saw-tooth design

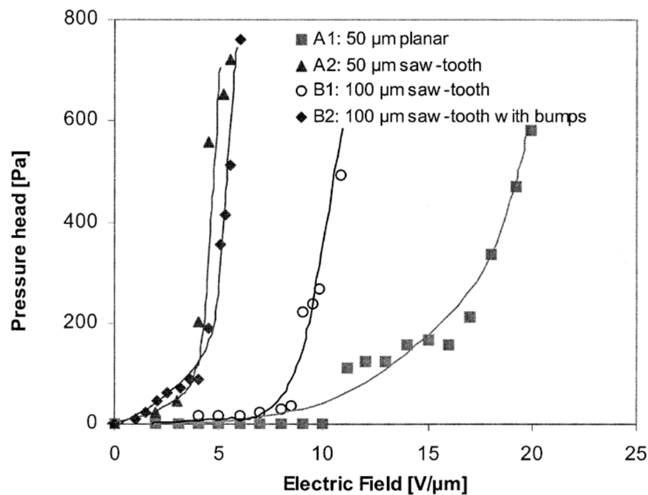


Fig. 9. Pressure head versus the electric field for various electrode designs.

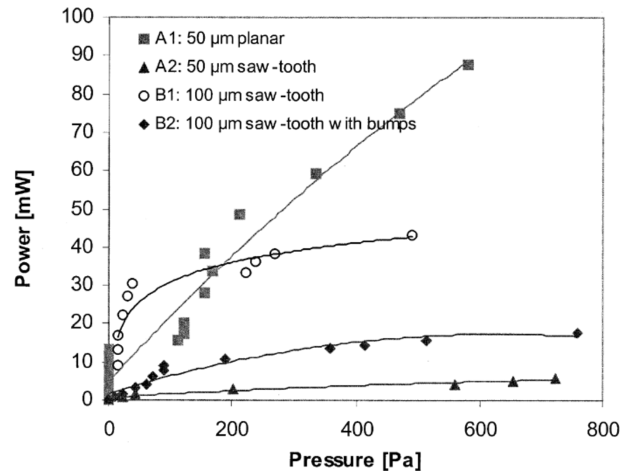


Fig. 10. Input electrical power consumption versus generated pumping pressure for various designs.

with bumps (A2) is more efficient than the 100 $\mu$m saw-tooth design without bumps (B2). Thus, it is expected that a 50-$\mu$m saw-tooth design with bumps to have a better performance than a 50-$\mu$m saw-tooth design without bumps. Indeed, one of our electrode designs included a 50-$\mu$m saw-tooth with bumps. However, this design was not testable due to some problem during its fabrication.

Another observation from these graphs is an abrupt increase in the pressure with increasing electric field. Generally, two different regions can be distinguished. At low electric field strengths, the pressure head is attributed to dissociation of impurities in the liquid. As the field strength increases, ions generated by dissociation of impurities are neutralized at the electrodes and the current density remains more or less independent of the electric field strength. At high electric field strengths, however, a steep increase in the pressure is observed. This is due to the charge injection at the electrodes. In the absence of impurities, the first region is unimportant, indicating that there is a threshold field strength below which no pumping is observed.

The rates of input electrical power consumption for the various micropumps as functions of pressure head for the various designs tested are shown in Fig. 10. As can be seen in this figure, the highest pumping efficiency is obtained for the saw-tooth design with the smallest electrode gap. This comparison also demonstrates that the design with bumps has a higher efficiency than one without bumps. The planar design requires the highest power input, which makes this design less efficient. As seen in Fig. 9, the electrode design A2 and B2 show a similar behavior in pressure head. However, the power consumptions for the electrode design A2 is lower. This is due to the fact that the electrode spacing is different in these two designs (50 $\mu$m for design A2 versus 100 $\mu$m for design B2). Thus, for a given electric field, the applied voltage in design A2 is approximately half that of the design B2, resulting in a lower power consumption.

## V. Conclusion

The feasibility of micropump fabrication using an array of 3-D bump structures was demonstrated and the pumping power generated by this micropump was quantified. We designed four ceramic devices and a series of patterned electrodes with different 3-D features that maximize the field gradients responsible for EHD pumping. The results were highly promising and demonstrated successfully the pumping capabilities of the micropump. The pump produced a pumping pressure of over 700 Pa using 3M's HFE-7100 thermal fluid. The results indicated that among the various designs that were tested, the saw-tooth geometry with 3-D bump structures performed the best. We believe reducing the electrode gap and increasing the number of pumping stages can further improve the pumping capability.

## Acknowledgment

The authors would like to thank TRW for their technical support and assistance in fabricating the devices. The efforts of A. Smith and G. Akerling of TRW were particularly instrumental in the successful fabrication of the micropumps.

## References

[1] O. M. Stuetzer, "Ion drag pressure generation," *J. Appl. Phys.*, vol. 30, no. 7, pp. 984–994, 1959.
[2] W. F. Pickard, "Ion-drag pumping: I theory," *J. Appl. Phys.*, vol. 34, no. 3, pp. 246–250, 1963.
[3] J. M. Crowley, G. S. Wright, and J. C. Chato, "Selecting a working fluid to increase the efficiency and flow rate of an EHD pump," *IEEE Trans. Ind. Appl.*, vol. 26, no. 1, pp. 42–49, 1990.
[4] J. E. Bryan and J. Seyed-Yagoobi, "An experimental investigation on Ion-drag pump in a vertical and axisymmetric configuration," *IEEE Trans. Ind. Appl.*, vol. 28, no. 2, pp. 310–316, 1992.
[5] G. Barbini and G. Coletti, "Influence of electrode geometry on ion-drag pump static pressure," *IEEE Trans. Dielect. Elect. Insul.*, vol. 2, no. 6, pp. 1100–1105, Dec. 1995.
[6] J. M. Crowley, *Fundamentals of Applied Electrostatics*. New York: Wiley, 1986, pp. 153–156.
[7] S. F. Bart, L. S. Tavrow, M. Mehregany, and J. H. Lang, "Microfabricated electrohydrodynamic pumps," *Sens. Actuators, Phys. A*, vol. 21, no. 1, pp. 193–197, 1990.
[8] A. Richter and H. Sandmaier, "An electrohydrodynamic pump," *IEEE Micro Electro Mechanical Systems: An Investigation of Micro Structures, Sensors, Actuators, Machines and Robots*, pp. 99–104, Feb. 1990.

[9] G. Fuhr, R. Hagedorn, T. Muller, and W. Benecke, "Microfabricated electrohydrodynamic (EHD) pumps for liquids of higher conductivity," *J. Microelectromech. Syst.*, vol. 1, pp. 141–146, Sept. 1992.
[10] S. H. Ahn and Y. K. Kim, "Fabrication and experiment of planar micro ion-drag pump," *Sens. Actuators, Phys. A*, vol. 70, pp. 1–5, 1998.
[11] J. Darabi, M. M. Ohadi, and D. DeVoe, "An electrohydrodynamic polarization micropump for electronic cooling," *J. Microelectromech. Syst.*, vol. 10, pp. 98–106, Mar. 2001.

**Jeff Darabi** (M'02) received the M.S. and Ph.D. degrees in mechanical engineering from the University of Maryland, College Park, in 1997 and 1999, respectively.

He is an Assistant Professor in the Department of Mechanical Engineering and Director of Microelectromechanical Systems (MEMS) Laboratory at the University of South Carolina, Columbia. His active research interests are in the areas of microelectromechanical systems (MEMS), microfluidic systems, and chip-integrated microcooling systems. He has pioneered several novel micropumps and microcooling devices for high heat flux electronic cooling applications. He is currently active in the development of chip-integrated micro cooling systems where he holds a related patent and micropumps for cooling spatially separate electronic components at cryogenic temperatures.

Dr. Darabi is a Member of the ASME and ASHRAE. He is the recipient of the Pi Tau Sigma Mechanical Engineering Professor of the Year Award (2001–2002), the Homer Addams Award (1999), the University of Maryland Outstanding Student Service Award (1999), and ASHRAE Grant-in-aid Fellowship (1995–1996 and 1998–1999).

**Mihai Rada** received the B.S. and M.S. degrees in Thermal Machines from the Polytechnique Institute of Bucharest, Romania. Currently, he is working towards the Ph.D. degree at the University of Maryland College Park.

His research interests focus on electrohydrodynamic pumping of cryogenic liquids, miniaturization of nonmechanical pumps, and cryogenic cooling systems.

**Michael Ohadi** received the Ph.D. degree in mechanical engineering from the University of Minnesota, Minneapolis, in 1986.

He is a Professor of Mechanical Engineering and Director of Small and Smart Thermal Systems Laboratory at the University of Maryland, College Park, and has more than 17 years of industrial and academic experience in the areas of thermal management and energy conversion. His most recent research has focused on active and hybrid augmentation of single-phase and phase-change heat and mass transfer with particular emphasis on use of the electrohydrodynamic (EHD) technique. His current research includes projects on development of miniaturized and intelligent thermal management systems with applications in commercial and defense thermal management and bio-microsystems. He directs the electronic cooling program at the Center for Electronic Products and Systems (CALCE) and is a Co-Director of Center for Environmental Energy Engineering (CEEE) at the University of Maryland. He has published extensively in his fields of expertise and is the recipient of several awards.

Dr. Ohadi is a Fellow of ASME and Associate Editor of two journals in his fields of expertise.

**John Lawler** received the Ph.D. degree in chemical engineering from the Massachusetts Institute of Technology (MIT), Cambridge.

Upon completion of his Ph.D., he studied polymer turbulent drag reduction at the Naval Research Laboratory. Currently, he is President and Technical Director at ATEC, Inc., College Park, MD, where he directs product development projects in the areas of micropumps, advanced electronic cooling techniques, and phase separation modules. Previously, he was a Staff Scientist at the corporate R&D centers of Hoechst Celanese Corporation and The Gillette Company.

Dr. Lawler is a Member of AIChE, ASME, and the Society of Rheology.